Enabling Force Sensing during Ground Locomotion: A bio-inspired, multi-axis, composite force sensor using discrete pressure mapping

Meng Yee (Michael) Chuah, and Sangbae Kim, *Member, IEEE*

***Abstract*—The paper presents a new force sensor design approach that maps the local sampling of pressure inside a composite polymeric footpad to forces in three axes, designed for running robots. Conventional multi-axis force sensors made of heavy metallic materials tend to be too bulky and heavy to be fitted in the feet of legged robots, and vulnerable to inertial noise upon high acceleration. To satisfy the requirements for high speed running, which include mitigating high impact forces, protecting the sensors from ground collision and enhancing traction, these stiff sensors should be paired with additional layers of durable, soft materials; but this also degrades the integrity of the foot structure. The proposed foot sensor is manufactured as a monolithic, composite structure composed of an array of barometric pressure sensors completely embedded in a protective polyurethane rubber layer. This composite architecture allow the layers to provide compliance and traction for foot collision while the deformation and the sampled pressure distribution of the structure can be mapped into three axis force measurement. Normal and shear forces can be measured upon contact with the ground, which causes the footpad to deform and change the readings of the individual pressure sensors in the array. A one-time training process using an artificial neural network is all that is necessary to relate the normal and shear forces with the multi-axis foot sensor output. The results show that the sensor can predict normal forces in the Z-axis up to 300N with a root mean squared error of 0.66% and up to 80N in the X- and Y-axis. The experiment results demonstrates a proof-of-concept for a lightweight, low cost, yet robust footpad sensor suitable for use in legged robots undergoing ground locomotion.**

***Index Terms*—Force measurement, Force sensors, Robot sensing systems, Sensor arrays, Tactile sensors, Artificial neural networks, Legged locomotion, Pressure gauges, Piezoresistive devices, Piezoresistance**

I. Introduction

HIGH speed running places great demands on the diverse capabilities of the foot. In animals, the foot serves several functions during locomotion that are unmatched by current mobile robots. Their feet can adapt to the contours of the ground and provide traction [1], [2], dampen out harmful shocks through the medial longitudinal arch [3], and sense the surface roughness and adapt to changes [4], [5]; making the biological feet well suited for moving at high speed over uneven terrain. The force sensor in the footpad should have a high dynamic range[1] in both normal and shear directions, to detect incipient slip and for the robot to implement corrective measures to remain upright [6]. However, while maintaining high force sensitivity, the foot still needs to absorb the shock from impact, protect its internals, create traction in uneven terrain, and be tough enough to withstand the repeated foot strikes during running [7], [8]. Also to reduce the burden on the leg actuators and to achieve higher energy efficiency, the foot should be lightweight to reduce the rotational inertia when the leg cycles at high speed during running [9]. This set of diverse requirements are not readily addressed by conventional sensing methodologies.

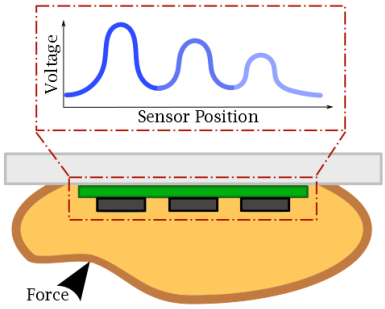

Fig. 1. **Deformation of elastomeric padding.** As ground reaction forces are applied to the footpad in this cross-sectional view, the soft elastomer deforms, sending a unique signal, based on the normal and shear components, to the barometric pressure sensor array PCB embedded within.

As a conventional approach, force/torque (F/T) sensors using strain gauges are commonly used to perform both feedback control and gait analysis in legged robots. However, these commercial sensors have limitations in highly dynamic applications. To measure ground reaction forces (GRFs), commercial F/T sensors are often used in series with a robot's feet, but at the cost of higher leg inertias and higher impact masses, making the robot less capable of dynamic motions. 'ASIMO' [10], 'KHR-3 Hubo' [11], 'iCub' [12], 'LOLA' [13], 'BHR-2' [8] and 'WABIAN-2' [14] are some examples of robots that incorporate a F/T sensor in each foot for sensing GRFs. The F/T sensor is either obtained commercially, or incorporated into the robot by measuring the deformation of rigid metal structures with semiconductor strain gauges [12]. However, the mass of the F/T sensor at the distal end of the leg significantly increases the leg inertia, and is prone to experiencing inertial noise during high impact and rapid movements, both of which occur all the time in running. In particular, the inertial noise is highly undesirable as it may produce false positives for the occurrence of ground contact, which may cause instabilities

The authors are with the Department of Mechanical Engineering, Massachusetts Institute of Technology, Cambridge, MA, 02139, USA. e-mail: mcx at mit.edu, Phone: 617-715-4309.

This work was supported by the Defense Advanced Research Projects Agency (DARPA) Maximum Mobility and Manipulation (M3) program.

Individual fellowship support was provided by the Agency for Science, Technology and Research (A*STAR) in Singapore.

[1]Dynamic range is defined as the ratio between the largest and smallest values of a signal.

in the system controller [15]. A typical commercial sensor will suffer from inertial noise under high acceleration and has been experimentally verified in a commercial F/T sensor under shaking.[2] Hence it is not viable to use F/T sensors for high speed locomotion and an alternative force sensing method is needed [16].

Researchers have attempted alternative methods of force sensing such as using force sensing resistors, contact switches or a combination of different sensors, but with limited degrees of success. Legged robots such as 'H6' and 'H7' [17], [18] use force sensing resistors (FSRs) to do force sensing in the foot, but this limits the GRFs measured to only the normal direction [19]. FSRs fail under large shear forces, so they still need to be protected when used in the foot. Some legged robots simplify things further by forgoing with force sensors completely and just making do with simple contact switches [20], [21]. This makes it hard to control the robot on surfaces where the friction differs from normal (i.e. on a wet or sandy floor with low friction or on inclined or uneven surfaces) [7]. Soft sensing techniques have been explored by Park et. al. in the form of a custom-built strain sensor developed for use in an active soft orthotic device [22]. This is combined with their hyperelastic pressure sensor [23] to form a soft artificial skin with conductive liquid metal channels capable of multi-modal sensing [24]. Similarly, the exoskeletal end-effectors embedded with optical fiber Bragg grating sensors allowed Park et al. to integrate sensing while minimizing the bulkiness of hardware [25]. Kuehn et al. emphasizes the importance of sensing in the foot, and hence their quadrupedal robot contains multiple sensors in the foot, such as a F/T sensor, an array of 49 FSRs, an accelerometer, an absolute angular encoder and a proximity distance sensor [26]. These sensors are used to measure GRFs and detect collisions. Nevertheless, this large number of sensors integrated in the foot reduces the structural integrity, drives up the cost of the robot, and still suffers from the inertial noise issues associated with the use of F/T sensors as described above. Therefore, there is still a need to develop a force sensor capable of measuring high loads accurately while undergoing high speed locomotion.

Current research in tactile sensing has resulted in both high force sensing in a single axis, as well as force sensing in multiple axes, but not in combination and not suitable for the needs fo high speed locomotion. Mei et al. have created a MEMS tactile sensor that is capable of measuring up to 50N in the vertical direction and $\pm$10N in the horizontal directions [27]. However, typical loads are much higher in legged animals [28] and robots. An example is the MIT Cheetah, a running robotic quadruped that currently reaches speeds of 22 km/h, seen in Fig. 2. In the foot of the MIT Cheetah, forces go up to 300N in the vertical direction and $\pm$60N in the horizontal directions in simulations [29]. A survey of multiple tactile sensors by Dahiya et al. [30] and a review by Yousef et al. [31] show that most tactile sensors are not capable of measuring forces above 10N. While this and other similar solutions are well suited for tactile sensing in robotic manipulators, there

[2]A demonstration of inertial noise in a commercial F/T sensor can be seen at http://www.youtube.com/watch?v=_6Rvv9s5hko

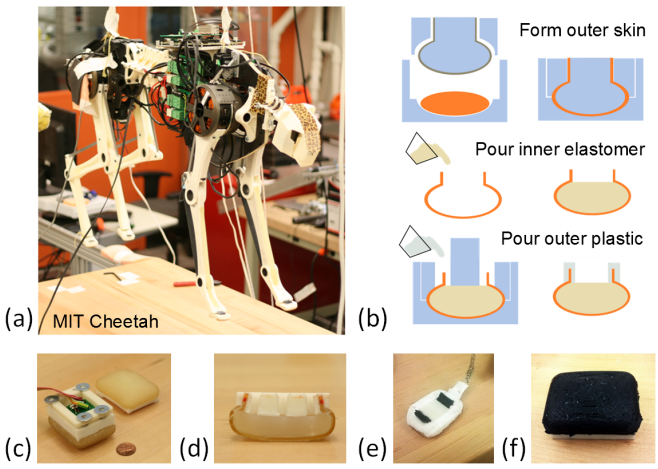

Fig. 2. **Prototype footpad iterations to achieved integrated force sensing in the foot of the MIT Cheetah.** (a) is a picture of the MIT Cheetah. (b) is the fabrication process of the composite foot. This work is further described in [16]. (c) is a prototype foot using magnets and Hall-effect sensors. (d) is a cutaway of another prototype foot using magnets and Hall-effect sensors. (e) is a prototype foot using FSR sensors. (f) is prototype foot using IR sensors.

is still much to be desired when considering the dynamic requirements of the foot on a running robot. It is desirable to extract only the essential measurements and minimize the demands put on the control system, which must compute the GRFs in real-time during running. It is interesting to note that Tajima et al. did not use force sensors in the feet of their humanoid robot precisely because of these difficulties [32].

The critical challenge here is to create a robotic foot that is compliant, robust and lightweight, while still being able to measure the large forces encountered in dynamic locomotion. It is also highly desirable to be able to measure forces in both the normal and shear directions, to construct the friction cone and detect slip during running.

To address these design challenges, we introduce a new approach to develop a lightweight, resilient force sensor suitable for use in high speed running robots, based on inspiration from biological skin. A number of mechanoreceptors (e.g. Ruffini endings, Merkel's discs and Meissner's corpuscles in the dermis layer.) [33] measure forces by multiplicity of sensing deformation and vibration of the skin layer, which also provide traction, compliance, and protection of the mechanoreceptors. Similarly, our footpad, represented in Fig. 1, has a compliant layer made out of polyurethane rubber and the local pressure distribution is sampled by an array of embedded pressure sensors.

The remainder of the paper explains the details of the sensing technique. Section II describes the design and fabrication of the foot with the embedded sensing technology. Section III describes how the foot sensor was characterized and calibrated, going into detail about how an artificial neural network was used to accurately obtain the force relationship of the foot sensor. Section IV discusses the challenges encountered and how future prototypes might be improved.

II. Multi-Axis Sensing Methodology

A. Sensor Array Design

To measure forces in both the normal and shear directions, the foot sensor utilizes the approach of embedding barometric pressure sensors within a layer of polyurethane rubber. The original purpose of these barometric pressure sensors are to measure atmospheric pressure changes, but in this case they have been re-purposed and embedded in an elastomer to be used for sensing force. A similar approach has been explored by researchers such as Zillich et al., who used a soft foam rubber with an embedded pressure sensor. Using just a single sensor, they have achieved high sensitivity in the order of tens of mNs in the normal direction [34]. Tenzer et al. have taken this concept and expanded it to make an open-source sensor array, called 'TakkTile', that communicates using the I^2C bus protocol for use in tactile sensing tasks [35]. In our foot sensor, a 3-by-3 array of high pressure sensors (Freescale Semiconductor MPXH6400A) is first mounted onto a custom printed circuit board (PCB) of size 40mm by 50mm (Fig. 3a). The port of each individual pressure sensor is cut open to expose more of the silicon piezoresistive transducer as seen in Fig. 3b. Each peripheral sensor is separated by a distance of 15mm in the X-axis and 10mm in the Y-axis. This orientation allows each sensor to pick up the slight changes in the pressure distribution within the polymer during ground contact. As the MIT Cheetah will be running on largely planar surfaces, the differences in pressure distribution are likely to arise due to shear forces. Using the pressure signals, these normal and shear forces will be reconstructed following the use of a neural network in Section III-C. On non-planar terrain, this assumption no longer holds and it would be difficult to resolve the normal and shear forces. The whole PCB is then embedded within a layer of polyurethane rubber that is in the shape of the desired footpad (Fig. 3c). As the pressure sensors are in direct contact with the elastomer, any forces on the foot are transmitted as strain in the elastomer and affects the individual pressure sensors differently. The signals from the pressure sensors are then collected and used to determine the original applied forces on the foot.

An additional benefit of using commercially available barometric pressure sensors is the low cost. The prototype foot sensor was made for less than $100 in parts and this price is expected to go down in volume. This makes it an attractive option as compared to a commercial force-torque sensor that can cost up to $10,000. As noted by Lee and Tiwana et al., the cost of current tactile sensors is one of the main reasons that they are not adopted in industrial and commercial products, especially health care and service robots [36], [37]. The cost effectiveness of our multi-axis force sensor makes it an attractive option for use in these aforementioned contexts.

B. Footpad Design and Fabrication

The design and fabrication of the footpad is vital to ensure that the footpad remains compliant enough to provide good traction with the ground, while robust enough to withstand the forces and wear and tear during ground locomotion. This current foot design has gone through multiple design iterations (as seen in Fig. 2) and has demonstrated robust performance with our MIT Cheetah, a quadrupedal robotic platform intended to test high speed running. The biomimetic design was inspired by the texture and shape of feline paws [1], [4]. The geometry of the base of these footpads are intentionally curved so as to amplify the differences in the pressure distribution and to avoid simple shear from occurring. This work serves to incorporate force sensing into the current design for measuring GRFs.

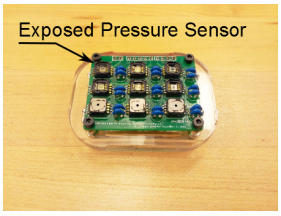

(a) Barometric pressure sensors soldered onto the PCB in a 3-by-3 array.

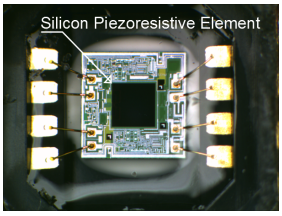

(b) Closeup view of the exposed silicon piezoresistive transducer within a barometric pressure sensor.

(c) Completed multi-axis force sensing footpad prototype.

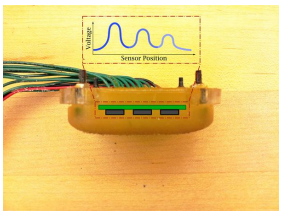

(d) Footpad prototype with graphical overlay showing where the pressure sensor array PCB is located.

Fig. 3. **Barometric pressure sensors used and completed force sensor.**

Several aspects were incorporated into the design of the foot in order to promote successful interaction with the ground. The footpad was fabricated by casting several different thermosetting polymers to one another. The monolithic design was chosen to promote robustness during impact, and minimize the size the sensing unit occupied. As an added bonus, since the sensor is completely encased in the footpad, it is protected from the environment and unlikely to fail. An illustrated overview of the process can be seen in Fig. 2. Firstly, the tough, outer "skin" of the foot was constructed by embedding woven fiberglass into a 2mm thick layer of Vytaflex® 20, a polyurethane rubber of Shore hardness 20A, in order to withstand the wear and tear that repeated impact and loading would impose on the material. The polyurethane rubber material provided a high coefficient of friction to generate sufficient forces tangent to the ground during contact. Sitti et al. has found that Vytaflex® 10 has a high static coefficient of friction of 2, due to the adhesion forces between the material and the tested acrylic surface [38]. As the MIT Cheetah is currently running on a treadmill, and will eventually be running outdoors, this increased traction is desirable to handle a variety of ground conditions. Woven fiberglass embedded within the outer, polyurethane rubber layer strengthen it against strain in the surface area of the pad. This resistivity to strain strengthens

the pad to shear forces but keeps the foot compliant to forces acting normal to its surface. This directional compliance further facilitates the driving mechanism utilized by the sensor, as the soft elastomer is prevented from slipping out from under the foot due to shear. The compliant pad also lowers peak forces experienced by the foot and acts as a mechanical, low-pass filter for asperities in the ground. The compliance allows the foot to simply deform around smaller asperities in the ground that would trouble rigid structures. After demolding, the skin retained the shape imposed by the casting process and was filled with Ecoflex® 00-10 Supersoft Silicone rubber of Shore hardness 00-10A, which was allowed to self-level. A rigid, outer lining was cast on top of these polyurethane rubbers using Task® 4 polyurethane resin of Shore hardness 83D. The rigid lining provided structural integrity and allowed for the PCB to be anchored onto the foot. This approach was used in the previous prototype footpad made with magnets and Hall-effect sensors, as described in [16]. The results in this paper are solely from the prototype footpad utilizing barometric pressure sensors.

This current prototype (Fig. 3c) using barometric pressure sensors is made with a layer of Vytaflex® 10. The next prototype would use the fabrication approach outlined above. The current prototype was made quickly as a proof-of-concept, and work is already underway to integrate the barometric pressure sensors into the more complex fabrication method as described in the previous paragraph. Integrating the foot sensor into the footpad means that the amount of mass in series with the sensing unit is kept to a minimum. In the current design, the foot sensor is very lightweight, only weighing 90g. This reduces unwanted dynamic effects which give rise to instabilities, such as inertial noise during periods of high acceleration. This commonly occurs in running robots performing dynamic locomotion.

In order to measure force, it must be converted into a quantity that can readily be measured as a signal. The deformation of the soft elastomer within the paw pad was chosen as the sensing mechanism. This required no additional mass to the foot other than embedding barometric pressure sensors into the structure. The chosen mechanism incorporates the compliance necessary to facilitate successful interaction with the terrain, and minimizes any additional weight or components, and allows for a monolithic and robust structure. The presented sensor strives to attain a greater level of integration within a compliant structure in order to preserve the original design intent and promote dynamics favorable to running while measuring ground reaction forces as close to the foot-ground interface as possible.

III. Sensor Characterization

In order to map the pressure signals to represent force data properly, it first needs to be characterized and calibrated. This section details the collection of the experimental data, several system identification approaches tested (AutoRegressive-moving-average model, Prediction-Error Model, and Artificial Neural Network) and the rationale behind choosing to implement an artificial neural network in the end.

(a) CNC milling machine with the footpad and F/T sensor mounted within.

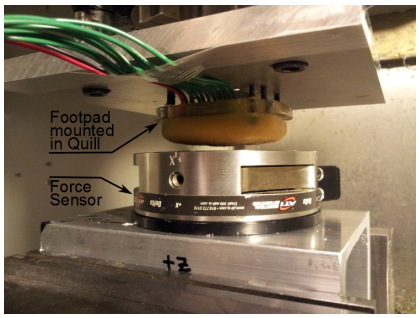

(b) A close-up of the footpad and F/T sensor before contact.

Fig. 4. **Experimental setup with the CNC milling machine.** The foot was mounted directly to the quill of the milling machine to ensure stiffness. The footpad made direct contact with the 6-axis force sensor during testing.

A. Experimental Setup

In order to get data to characterize the sensor, accurate linear positioning of the footpad is required in both normal and shear directions. This was achieved by using an industrial 3 axis CNC milling machine (HAAS Super Mini Mill 2). A mount was fabricated to attach the footpad directly to the quill and a separate mount for attaching a 6-axis F/T sensor (ATI Industrial Automation SI-660-60) to the mill table. This experimental setup is shown in Fig. 4. The data from the foot sensor and the F/T sensor are acquired through a National Instruments (NI) CompactDAQ 9205 connected through LabVIEW. The data is then further processed in MATLAB™. The input data needs to be persistently exciting[3] enough in order to be informative enough to distinguish any two models from each other. To this end, a swept sine signal is commanded to the CNC mill in each of the 3 axes (i.e. X-, Y-, and Z-axis). The data was first collected by having the CNC milling machine run through a programmed path with

[3]Persistent excitation is defined here as the quality of an input signal to be able to excite all the modes of the system to be identified to assure the convergence of the parameters to their true values.

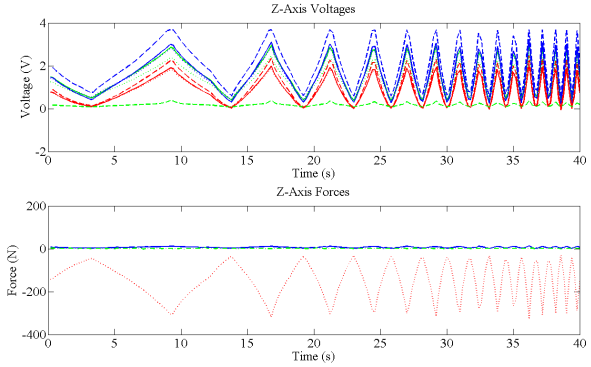

Fig. 5. **Swept Sine Data in Z-axis.** The top graph shows the output voltages from the array of barometric sensors embedded in the footpad. The bottom graph shows the forces recorded from the 6-axis F/T sensor (mounted beneath). The red line represents the Z-axis force data.

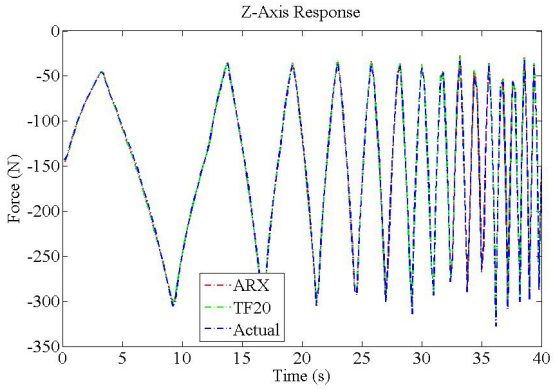

Fig. 6. **Comparison of the Z-axis models with the actual data.** The graph shows the comparison between a 2nd order transfer function model, a 4th order ARX model and the actual data. Note that since the models predict the actual data so well, the plots overlap each other and are hard to distinguish.

the footpad in contact with the F/T sensor. With a known normal load, the footpad was made to traverse 3mm in both the positive and negative directions along the X-axis. This was then repeated in the Y-axis. The Z-axis traverses only 1mm in displacement, but this is enough to generate a large change in normal forces. In the context of the MIT Cheetah, the Z-axis would correspond to the normal direction (i.e. the direction of the acceleration due to gravity), and the X-axis would correspond to the direction of forward motion of the MIT Cheetah. The swept sine signal is limited to a conservative 900mm/min in order to not damage the CNC mill. This data was found to be persistently exciting of order 50 in each of the 3 axes.

B. System Identification

The resulting voltages of the footpad from the Z-axis swept sine input showed that the sensors had repeatable output, with the peaks of each pressure sensor reaching the same level each time. The forces in the Z-axis range from 0 to 300N. This is shown in Fig. 5. Since the individual sensor readings exhibit the same trend, it is more efficient to use the average of the nine readings as an ensemble mean to represent the data in the Z-axis.

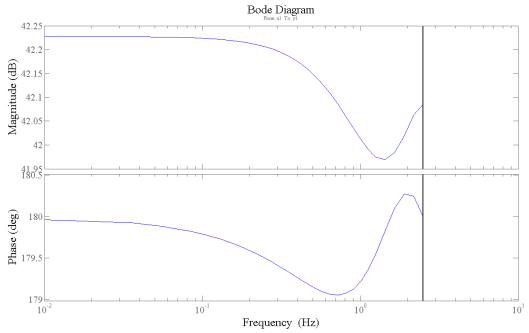

Fig. 7. **Bode Plot of 2nd order transfer function for the Z-axis.** The bode plot shows very little change in the magnitude as well as the phase.

A variety of models were applied using the System Identification Toolbox in MATLAB™ and the best models shown here. Both the transfer function estimation and a 4th order AutoRegressive-moving-average (ARX) model gave good results. A 2nd order transfer function estimation model gave the best result, with a root mean squared error (RMSE) of only 2.44N, an Akaike's Information Criterion (AIC) of 1.84 and a normalized RMSE (NRMSE) fitness value of 97.2%. The results of the models as compared to the actual data are plotted in Fig. 6. The RMSE, AIC [39] and NRMSE fitness values are found using the following formulae

$$RMSE = \left[\frac{1}{N}\sum_{i=1}^{N}(\hat{y}_i - y_i)^2\right]^{\frac{1}{2}} \tag{1}$$

$$AIC = -2\log\{L[\hat{\theta}|y]\} + 2d \tag{2}$$

$$NRMSE = \left(1 - \frac{\|\hat{y}_i - y_i\|}{\|y_i - \bar{y}\|}\right) * 100\% \tag{3}$$

The 2nd order transfer function obtained is shown and it shows that in the Z-axis, the footpad behaves as a mass-spring-damper system. The bode plot of this 2nd order transfer function is plotted in Fig. 7.

$$G(z) = \frac{-126.8}{1 - 0.008069z^{-1} - 0.01041z^{-2}} \tag{4}$$

The Y-axis results are much less accurate than the Z-axis results, even though the individual signals were used instead of the ensemble mean. The resulting voltages of the footpad from the Y-axis swept sine input is shown in Fig. 8. The forces in the Y-axis range from -80N to +80N. Since the individual sensor readings show different behaviors, this becomes a multivariate system identification problem. In this case, the best option was to use a 4th order Prediction-Error Model (PEM). This resulted in a RMSE of 14.12N, an AIC of 4.22 and a NRMSE fitness value of 71.72%. The plot shows the comparison between the model and actual data (Fig. 9).

The X-axis results are largely similar to those of the Y-axis, but with a higher level of accuracy. The resulting voltages of the footpad from the X-axis swept sine input is shown in Fig. 10. The forces in the X-axis range from -80N to +80N. Similar to the Y-axis, the individual sensor signals are unique

and hence a multivariate model is sought. A 5th order PEM was found to minimize the errors. This is one order higher than that the optimal one found for the Y-axis data. The 5th order PEM produced a RMSE of 7.61N, an AIC of 4.63 and a NRMSE fitness value of 85.21%. These are all better values compared to those of the Y-axis model. This could be due to the difference in spacing of the barometric pressure sensors in the X- and Y-axis. As mentioned in Section II-A, the spacing between sensing elements is 15mm in the X-axis and only 10mm in the Y-axis. The plot shows the comparison between the model and actual data (Fig. 11).

C. Artificial Neural Network

Due to the complexity in the geometry of the footpad and the elastomer, attaining analytical models through the use of hyperelastic material models is non-trivial. The total force can be estimated by assuming that the footpad is a rectangular block of elastomeric material with various material models such as Mooney-Rivlin [40], Arruda-Boyce [41] and Ogden [42], but these models are highly dependent on the quality of the experimental data collected. The difficulty is furthered with the use of an elastomer (Vytaflex® 10) and the complex geometric boundary condition around the pressure sensor. This makes it almost impossible to accurately predict the actual pressure distribution in the footpad. Simulating the footpad deformations using a finite-element analysis package such as Abaqus™ was considered, but the resulting model was overly complex yet inaccurate. The footpad is essentially a Multiple Inputs, Multiple Outputs (MIMO) system, with the multiple inputs being the nine barometric pressure sensor signals, and the multiple outputs being the desired force predictions in the 3 axes. As shown in Section III-B, even using system identification techniques for each axis individually as a Multiple Inputs, Single Output (MISO) system presented difficulties. In the end, the use of an artificial neural network (ANN) to directly associate the forces with the pressure sensor readings was determined to be the best way to obtain the correlation. By training the neural network, the system transfer function of the foot sensor is approximated over particular regions of the state space. This creates a mapping that encompasses the non-linearity between the sensor output and the multi-axis force data. Lu et al. has explored using ANN for strain gauge to force/torque calibrations [43]. It offers the advantages of only requiring a one-time calibration procedure and is able to provide force feedback to the system in real-time. The basic procedure is show in the flow diagram in Fig. 12.

As described in Section II-A, a small 40mm by 50mm PCB

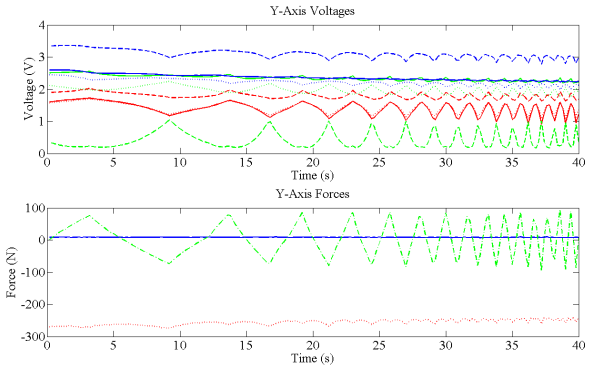

Fig. 8. **Swept Sine Data in Y-axis.** The top graph shows the output voltages from the array of barometric sensors embedded in the footpad. The bottom graph shows the forces recorded from the 6-axis F/T sensor. The green line represents the Y-axis force data.

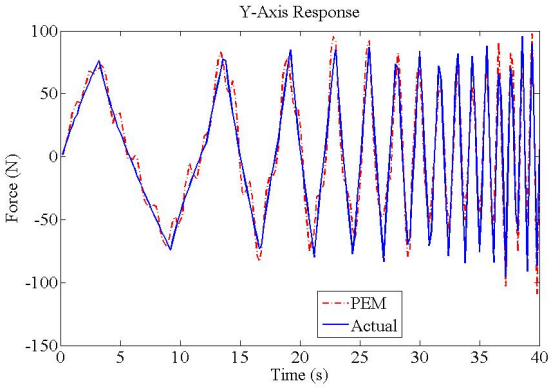

Fig. 9. **Comparison of the Y-axis models with the actual data.** The graph shows the comparison between a 4th order PEM model and the actual data.

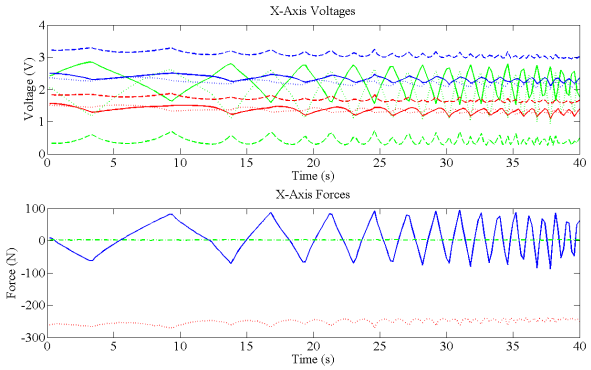

Fig. 10. **Swept Sine Data in X-axis.** The top graph shows the output voltages from the array of barometric sensors embedded in the footpad. The bottom graph shows the forces recorded from the 6-axis F/T sensor. The blue line represents the X-axis force data.

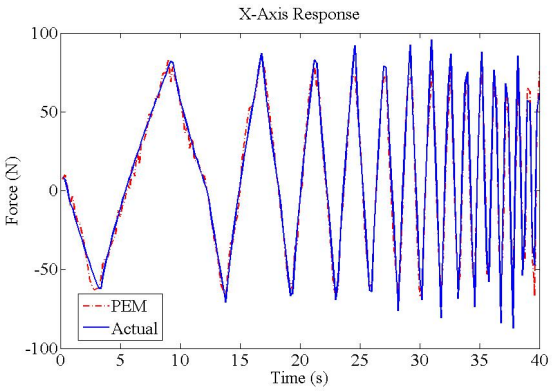

Fig. 11. **Comparison of the X-axis models with the actual data.** The graph shows the comparison between a 5th order PEM model and the actual data.

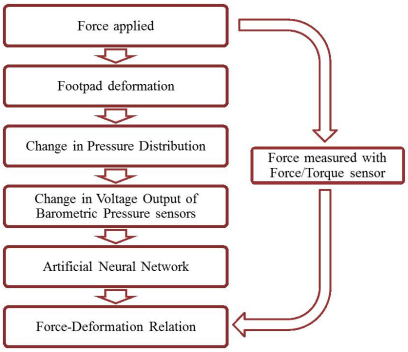

Fig. 12. **Neural Network Training Procedure.** The flow chart shows how the artificial neural network is trained with data from the F/T sensor.

was designed and manufactured and populated with a 3 by 3 array of barometric pressure sensors. The voltage readings are measured by the NI CompactDAQ 9205 and represented as 9 individual signals ($S_0, S_1, S_2, S_3, S_4, S_5, S_6, S_7$, and S_8). The overall change in the sensor array signal distribution can be summarized by the function:

$$S_{pressure}(t) = [S_0(t) \dots S_i(t) \dots S_8(t)]^T \tag{5}$$

where S_i is the individually measured voltage signal of the i^{th} pressure sensor. This PCB is then embedded in the polyurethane rubber layer of 10mm thickness. However, in the case of shear forces, the pressure signals along the outer edges change by different amounts and these discrepancies are picked up by the pressure sensors on the PCB.

The loading conditions on the footpad are measured by a F/T sensor and can be represented as:

$$F(t) = [F_X(t)\ F_Y(t)\ F_Z(t)]^T \tag{6}$$

where $F_i(t)$ is the recorded force in each respective axis.

This change in the pressure distribution, $S_{pressure}(t)$ is then parsed in MATLAB™ and the pressure distribution and the applied forces are empirically correlated using the Neural Network Toolbox. A feed-forward neural network is created where an input-output relationship is mapped between the pressure distribution as measured by the 9 barometric pressure sensors and the 3 axis forces recorded by the F/T sensor. The Levenberg-Marquardt optimization network training function [44] then uses a back-propagation algorithm to update the weights and bias values of the neural network until the minimum mean squared error is obtained and the desired performance is realized. Note that the Levenberg-Marquardt algorithm, or damped least-squares method, is an example of a nonlinear regression algorithm. The Levenberg-Marquardt algorithm is given as:

$$[J^T W J + \lambda \text{diag}(J^T W J)]\delta = J^T W [F(t) - \hat{F}(t)] \tag{7}$$

where J is the Jacobian matrix, W is the weighting matrix, λ is the algorithmic parameter, δ is the increment in each iteration, $F(t)$ is the target force output from the F/T sensor and $\hat{F}(t)$ denotes the force estimates of the ANN. This method

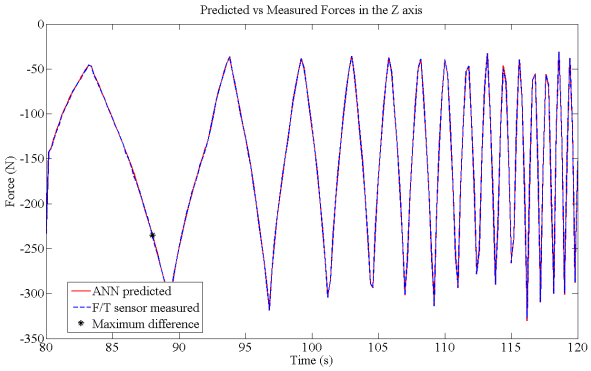

(a) Predicted vs Measured Forces in the Z-Axis

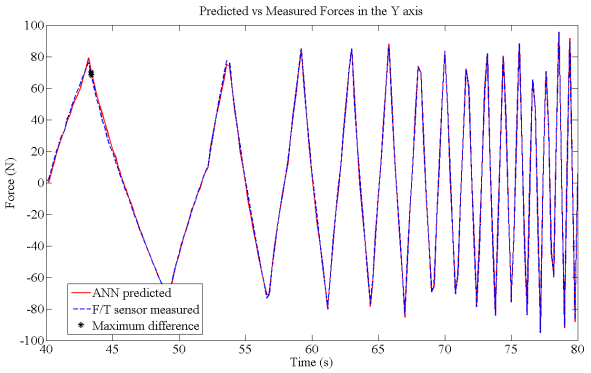

(b) Predicted vs Measured Forces in the Y-Axis

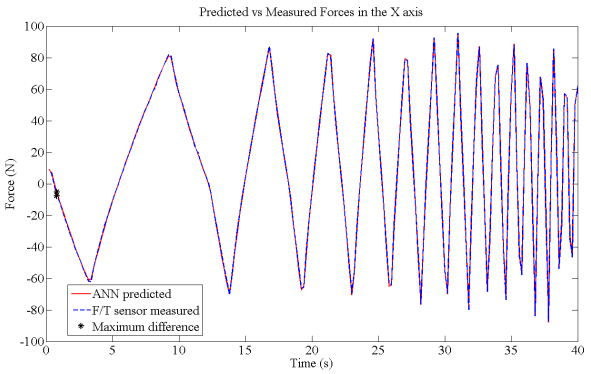

(c) Predicted vs Measured Forces in the X-Axis

Fig. 13. **Experimental results for correspondence between the predicted force and actual force.** The blue line shows the actual force measured and the red line shows the neural network predicted force.

on the use of artificial neural networks for force sensing is based on work done by Ananthanarayanan et al. [45]. Using the combined swept sine data collected previously, a 10 neuron neural network was trained and the resulting comparison between the predicted output and actual output is shown in Fig. 13. For the Z-axis, the RMSE was only 0.69N and the maximum deviation was only 1.85N when the data ranged from 50N to 300N. Similarly, the Y-axis and X-axis results were equally impressive, with the RMSE being 1.23N and 0.92N and a maximum deviation 2.60N and 2.86N respectively, out of a range of $\pm$80N.

Since the artificial neural network showed the best per-

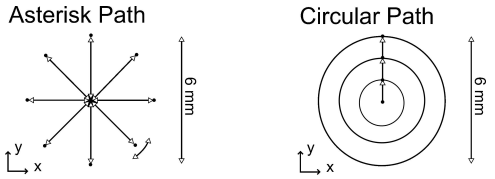

(a) **Training Paths.** The two paths above were used to train the ANN.

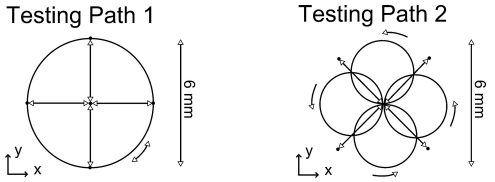

(b) **Testing Paths.** The two paths above were used to test the ANN.

Fig. 14. Training and testing paths used to collect the data needed for the ANN. The furthest points on each sub-trajectory correspond to a radius of 3mm away from the center of each path. Both paths were run at several, set normal displacements in the Z-axis.

TABLE I
SUMMARY OF THE EXPERIMENTAL RESULTS. THE MAXIMUM FORCE, RMSE AND MAXIMUM ERROR BETWEEN THE PREDICTED FORCES AND ACTUAL FORCES AS MEASURED BY THE F/T SENSOR IS SHOWN.

Force Sensor	Maximum Force			RMS Error			Maximum Error		
	Z-axis	Y-axis	X-axis	Z-axis	Y-axis	X-axis	Z-axis	Y-axis	X-axis
Pressure	300 N	80 N	80 N	1.98 N 0.66 %	4.73 N 5.91 %	2.95 N 3.69 %	14.95 N 4.99 %	23.14 N 28.92 %	14.90 N 18.62 %

formance when compared to the linear system identifications methods in minimizing the RMSE, more training and testing data was collected for use with the artificial neural network and further verification. Training data was first collected by having the CNC milling machine run through a programmed training path with the footpad in contact with the F/T sensor. Under a range of displacements in Z-axis up to 1.5mm with steps of 0.1mm, the footpad was made to follow the 'asterisk path' and 'circular path' as shown in Fig. 14a. The 'asterisk path' starts from the origin and traverses 3mm in 45 degree intervals until a full revolution is made. The 'circular path' involves the footpad traversing a 2mm, then 4mm, and finally a 6mm diameter circle in both clockwise and counter-clockwise directions.

For verification, the more data was gathered with two arbitrary testing paths. The first testing path involves the footpad moving 3mm in both the positive and negative X-axis direction, followed by the Y-axis direction and ending with it traversing a circular path of 6mm diameter clockwise and then counter-clockwise. The second testing path involved a diagonal motion of 3mm in each of the 4 quadrants of the X and Y-axis. This was then followed with 4 smaller circular paths of 3mm diameter along each of the positive and negative X and Y-axis. A qualitative depiction of the testing paths is shown in Fig. 14b.

Once the artificial neural network is trained, the network is simulated with the testing data and the predicted results are plotted together with the actual forces experienced by the

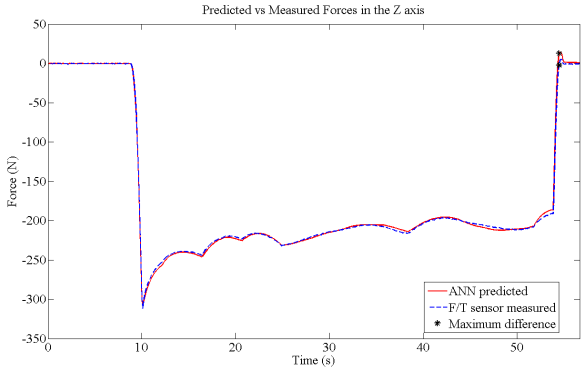

(a) Predicted vs Measured Forces in the Z-Axis

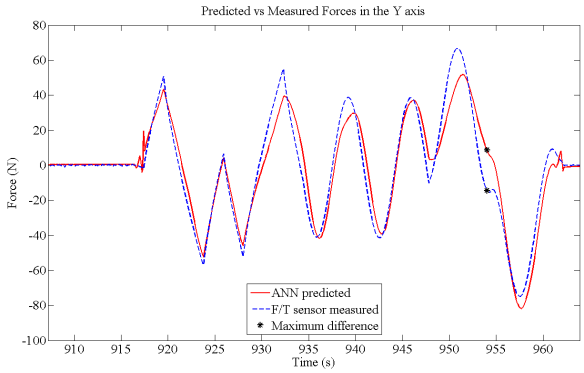

(b) Predicted vs Measured Forces in the Y-Axis

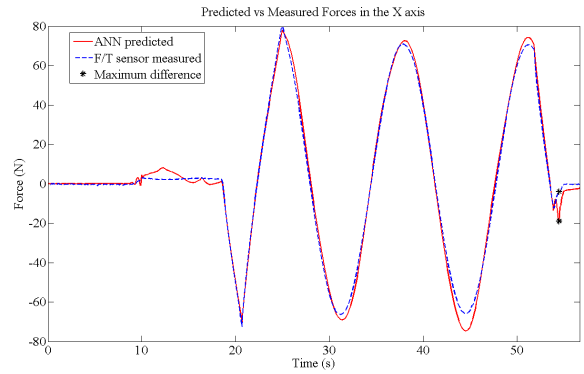

(c) Predicted vs Measured Forces in the X-Axis

Fig. 15. **Experimental results for correspondence between the predicted force and actual force.** The blue line shows the actual force measured and the red line shows the neural network predicted force. Note that each plot only shows one cycle of the testing paths.

footpad during the testing phase. The results (Fig. 15) show that the neural network is able to predict normal forces in the Z-axis up to 300N with the greatest accuracy with an RMSE of only 1.98N. This is followed by the X-axis where shear forces of 80N are measured and the RMSE is only 2.95N. In the Y-axis, similar performance is observed where shear forces of up to 80N are predictable, with a RMSE of 4.73N. These results are summarized in Table 1. With the trained neural network stored, the signals for the barometric pressure sensor array can be simulated and the forces in three axes obtained in real-time. Experimentally, peak forces above 400N have been

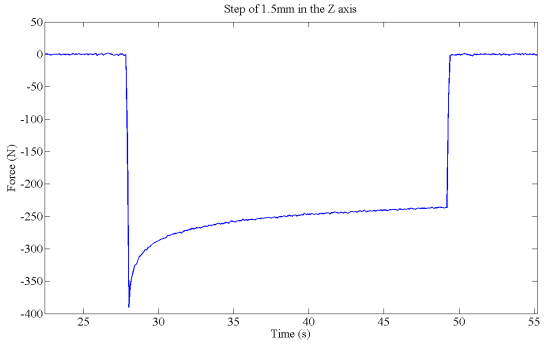

Fig. 16. **Stress Relaxation in the Z-axis.** The blue line shows the actual force measured in the Z-axis when subjected to a displacement step of 1.5mm The force increases to almost 400N before relaxing back to 250N without any change in displacement.

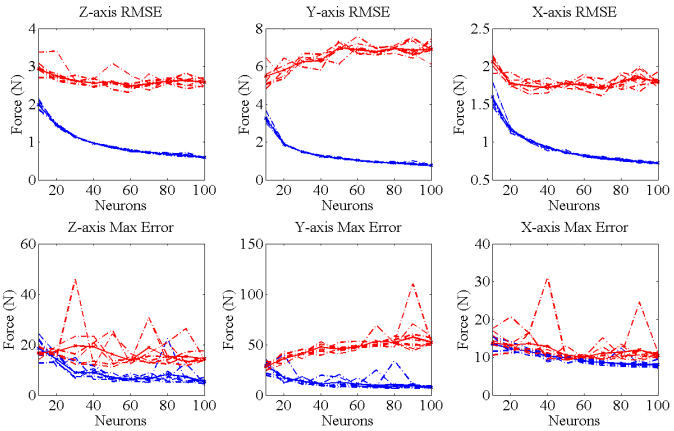

Fig. 17. **Investigation of the Effect of Additional Neurons.** The top row shows the RMSE plots and the bottom row the maximum error. The leftmost column represents the Z-axis data, the middle the Y-axis data and the rightmost the X-axis data. The blue lines show the training data and the red lines show the testing data for 10 trials.

observed for the Z-axis and forces in the X- and Y-axis have reached 100N maximally during tests.

IV. Discussion and Future Works

The end goal is to have sensing capabilities were efficiently integrated to the structure with minimal addition of hardware, but several aspects of the design are readily available for possible improvement. In the case of the MIT Cheetah, a proven foot using this fabrication structure had already been developed and utilized in currently running experiments (Fig. 3). The experimental results show that the footpad sensor is able to detect normal loading conditions in the Z-axis and shear in both the X- and Y-axis with great accuracy. This can be used to detect when slipping occurs between the foot of the robot and the ground, and corrective measures can be taken. These results present a promising proof-of-concept on a novel mechanism to sense ground reaction forces while utilizing an inherently compliant interface with the terrain. While this has been achieved in the current prototype, other improvements could be made with further investigation.

Collecting additional training data may further fine-tune the ANN parameters and will allow us to minimize the errors in the force sensing. Only a few trajectories, repeated at varying normal loads, was used to produce the current correlation. There might be some load history dependence (e.g. stress relaxation and hysteresis) which needs to be investigated further. Stress relaxation effect can be seen taking place in Fig. 16, where the measured Z-axis force drops from 400N to 250N without any change in displacement. Specifically, impact tests may prove to be the most relevant training method for running and would provide more telling information. However the short duration of ground contact in running robots (about 120ms in our experiments) might make this a moot point. The effect of impact is currently under investigation. A new footpad design has been fabricated and attached to the MIT Cheetah. Tests are underway to establish the reliability of the new footpad sensor in high speed locomotion.

There is a trade-off between increasing the number of neurons used in the artificial neural network to improve the accuracy and the associated danger of overfitting the ANN to the training data. To investigate this, the training is repeated for neural networks of 10 to 100 neurons and each time the training is further repeated for ten trials each. The results are shown in Fig. 17. The blue lines show the RMSE and maximum error of the training data of the ten trials as the number of neurons increase from 10 to 100. The red lines represent the testing data. The trials show that while the RMSE and maximum error decreases as expected with increasing number of neurons for the training data, the testing data does not show a similar trend of benefiting from additional neurons. This is especially the case for the Y-axis testing data where the RMSE and maximum error actually increases for increasing number of neurons.

In order to further improve the measurement of shear forces, the number of sensors and alternative placement of the barometric pressure sensors is currently being further explored. Rather than having the pressure sensors spaced regularly, an irregular spatial arrangement or circular orientation may increase sensitivity and accuracy to shear forces. The minimum number of sensing elements that is needed to detect forces in three axes is being investigated in hopes of reducing the overall footprint.

A combination of pressure sensors with different sensing ranges could be used together in a single footpad to achieve a greater dynamic range in force measurement. In the human skin, there are four main types of mechanoreceptors (i.e. Ruffini's end organs, Meissner's corpuscles, Pacinian corpuscles and Merkel's discs). These mechanoreceptors each perform a different role, enabling the skin to differentiate between a wide variety of forces and textures [33]. By varying the pressure range and types of the barometric pressure sensors used in the sensor array, as well as the material properties of the elastomer, a similar effect can be achieved. This can be incorporated into the current '2-pad' design (Fig. 2) where a single foot will have 2 gel-like footpads of different stiffness. This will allow the MIT Cheetah foot to measure a wider dynamic force range.

In the next prototype, a microcontroller and additional

Analog-to-Digital Converter (ADC) microchips would be able to directly process the voltage signals from the barometric pressure sensor array onboard and send out the predicted multi-axis forces. This could be done with SPI communications for high bandwidth. Bluetooth or WiFi communications could also be utilized to transmit the data and make the foot sensor a truly 'intelligent sensor' [46].

V. Conclusion

During running, the foot of a legged robot hits the ground multiple times with large forces, introducing undesirable effects such as inertial noise that make it difficult to detect ground contact. Current sensors are not suitable for measuring ground reaction forces because of these problematic effects. This paper presents a footpad with integrated force sensing capabilities that addresses these issues in ground locomotion. Ground reaction forces can be accurately measured during ground locomotion, allowing a robot to react to changing terrain and incipient slip. The foot is made of a polyurethane rubber with an embedded array of barometric pressure sensors, which allows normal and shear forces to be detected indirectly without the need to expose the sensor. The elastomer covering the pressure sensor array also provides durability under repeated impacts while still being compliant enough to offer good traction. A one-time training process using an artificial neural network is all that is necessary to relate the normal and shear forces with the foot sensor output. The multi-axis foot sensor is able to detect large normal forces up to 300N with a RMSE of 0.66% and up to $\pm$80N in the X and Y-axis with an RMSE of 3.69% and 5.91% respectively. Peak forces of 400N in the normal direction, and $\pm$100N in the shear directions were observed during tests. This is a lightweight ($<$100g) and low cost ($<$\$100), robust footpad sensor suitable for use in robots performing locomotion to detect the occurrence of ground contact and the ground reaction forces involved.

Acknowledgment

The authors of this paper would like to thank Albert Wang and Sangok Seok of the Biomimetic Robotics Laboratory for their help with the experimental setup and LabVIEW data acquisition. This work was supported by the Defense Advanced Research Projects Agency (DARPA) Maximum Mobility and Manipulation (M3) program. Individual fellowship support was provided by the Agency for Science, Technology and Research (A*STAR).

References

[1] R. M. Alexander, M. B. Bennett, and R. F. Ker, "Mechanical properties and function of the paw pads of some mammals," *Journal of Zoology*, vol. 209, no. 3, pp. 405–419, 1986.

[2] R. F. Ker, M. B. Bennett, S. R. Bibby, R. C. Kester, and R. M. Alexander, "The spring in the arch of the human foot." *Nature*, vol. 325, pp. 147–149, Jan. 1987.

[3] S. G. M. Humphry, *The human foot and the human hand*. Macmillan, 1861.

[4] S. Davis and D. G. Caldwell, "The design of an anthropomorphic dexterous humanoid foot," in *2010 IEEE/RSJ International Conference on Intelligent Robots and Systems (IROS)*, 2010, pp. 2200–2205.

[5] L. Klenerman, B. Wood, and N. Griffin, *The Human Foot: A Companion to Clinical Studies*. Springer, 2006.

[6] M. T. Francomano, D. Accoto, and E. Guglielmelli, "Artificial Sense of Slip - A Review," *Sensors Journal, IEEE*, vol. 13, no. 7, pp. 2489–2498, 2013.

[7] K. Kaneko, F. Kanehiro, S. Kajita, M. Morisawa, K. Fujiwara, K. Harada, and H. Hirukawa, "Slip observer for walking on a low friction floor," *2005 IEEE/RSJ International Conference on Intelligent Robots and Systems (IROS)*, pp. 634–640, 2005.

[8] J. Li, Q. Huang, W. Zhang, Z. Yu, and K. Li, "Flexible foot design for a humanoid robot," *2008 IEEE International Conference on Automation and Logistics (ICAL)*, no. September, pp. 1414–1419, 2008.

[9] S. Seok, A. Wang, M. Y. Chuah, D. Otten, J. Lang, and S. Kim, "Design principles for highly efficient quadrupeds and implementation on the mit cheetah robot," in *Robotics and Automation (ICRA), 2013 IEEE International Conference on*, May 2013, pp. 3307–3312.

[10] K. Hirai, M. Hirose, Y. Haikawa, and T. Takenaka, "The development of Honda humanoid robot," *1998 IEEE International Conference on Robotics and Automation (ICRA)*, vol. 2, pp. 1321–1326, 1998.

[11] I.-W. Park, J.-Y. Kim, J. Lee, and J.-H. Oh, "Mechanical design of humanoid robot platform KHR-3 (KAIST humanoid robot 3: HUBO)," in *2005 5th IEEE-RAS International Conference on Humanoid Robots*, vol. 3, 2005, pp. 321–326.

[12] N. G. Tsagarakis, G. Metta, G. Sandini, D. Vernon, R. Beira, F. Becchi, L. Righetti, J. Santos-Victor, A. J. Ijspeert, M. C. Carrozza, and D. G. Caldwell, "iCub: the design and realization of an open humanoid platform for cognitive and neuroscience research," *Advanced Robotics*, vol. 21, no. 10, pp. 1151–1175, 2007.

[13] S. Lohmeier, T. Buschmann, and H. Ulbrich, "System design and control of anthropomorphic walking robot LOLA," *IEEE/ASME Transactions on Mechatronics*, vol. 14, no. 6, pp. 658–666, 2009.

[14] Y. Ogura, K. Shimomura, A. Kondo, A. Morishima, T. Okubo, S. Momoki, and A. Takanishi, "Human-like walking with knee stretched, heel-contact and toe-off motion by a humanoid robot," *2006 IEEE/RSJ International Conference on Intelligent Robots and Systems (IROS)*, pp. 3976–3981, Oct. 2006.

[15] S. Eppinger and W. Seering, "Three dynamic problems in robot force control," *1989 IEEE International Conference on Robotics and Automation (ICRA)*, vol. 1, pp. 392–397, May 1989.

[16] M. Y. M. Chuah, M. Estrada, and S. Kim, "Composite force sensing foot utilizing volumetric displacement of a hyperelastic polymer," *2012 IEEE/RSJ International Conference on Intelligent Robots and Systems (IROS)*, pp. 1963–1969, Oct. 2012.

[17] K. Nishiwaki, T. Sugihara, S. Kagami, F. Kanehiro, M. Inaba, and H. Inoue, "Design and development of research platform for perception-action integration in humanoid robot: H6," *2000 IEEE/RSJ International Conference on Intelligent Robots and Systems (IROS)*, vol. 3, pp. 1559–1564, 2000.

[18] K. Nishiwaki, J. Kuffner, S. Kagami, M. Inaba, and H. Inoue, "The experimental humanoid robot H7: a research platform for autonomous behaviour." *Philosophical Transactions of the Royal Society A: Mathematical, Physical and Engineering Sciences*, vol. 365, no. 1850, pp. 79–107, Jan. 2007.

[19] Y.-D. Kim, B.-J. Lee, J.-H. Ryu, and J.-H. Kim, "Landing Force Control for Humanoid Robot by Time-Domain Passivity Approach," *IEEE Transactions on Robotics*, vol. 23, no. 6, pp. 1294–1301, Dec. 2007.

[20] C. Chevallereau, A. Gabriel, Y. Aoustin, F. Plestan, E. Westervelt, C. C. De Wit, and J. Grizzle, "Rabbit: A testbed for advanced control theory," *IEEE Control Systems Magazine*, vol. 23, no. 5, pp. 57–79, 2003.

[21] S. Talebi, I. Poulakakis, E. Papadopoulos, and M. Buehler, "Quadruped robot running with a bounding gait," in *Experimental Robotics VII*, D. Rus and S. Singh, Eds. Springer Berlin Heidelberg, 2001, pp. 281–289.

[22] Y.-L. Park, B.-r. Chen, D. Young, L. Stirling, R. J. Wood, E. Goldfield, and R. Nagpal, "Bio-inspired active soft orthotic device for ankle foot pathologies," in *Intelligent Robots and Systems (IROS), 2011 IEEE/RSJ International Conference on*, 2011, pp. 4488–4495.

[23] Y.-L. Park, C. Majidi, R. Kramer, P. Bérard, and R. J. Wood, "Hyperelastic pressure sensing with a liquid-embedded elastomer," *Journal of Micromechanics and Microengineering*, vol. 20, no. 12, p. 125029, 2010.

[24] Y.-L. Park, B.-r. Chen, and R. J. Wood, "Soft artificial skin with multimodal sensing capability using embedded liquid conductors," in *Sensors, 2011 IEEE*, 2011, pp. 81–84.

[25] Y.-L. Park, S. C. Ryu, R. Black, K. Chau, B. Moslehi, and M. Cutkosky, "Exoskeletal force-sensing end-effectors with embedded optical fiber-

bragg-grating sensors," *Robotics, IEEE Transactions on*, vol. 25, no. 6, pp. 1319–1331, 2009.
[26] D. Kuehn, F. Grimminger, F. Beinersdorf, F. Bernhard, A. Burchardt, M. Schilling, M. Simnofske, T. Stark, M. Zenzes, and F. Kirchner, "Additional dofs and sensors for bio-inspired locomotion: Towards active spine, ankle joints, and feet for a quadruped robot," in *Robotics and Biomimetics (ROBIO), 2011 IEEE International Conference on*, Dec 2011, pp. 2780–2786.
[27] T. Mei, W. J. Li, Y. Ge, Y. Chen, L. Ni, and M. H. Chan, "An integrated MEMS three-dimensional tactile sensor with large force range," *Sensors and Actuators A: Physical*, vol. 80, no. 2, pp. 155–162, Mar. 2000.
[28] R. M. Walter and D. R. Carrier, "Ground forces applied by galloping dogs," *Journal of Experimental Biology*, vol. 210, no. 2, pp. 208–216, Jan. 2007.
[29] H.-W. Park and S. Kim, "Variable Speed Galloping Control using Vertical Impulse Modulation for Quadruped Robots: Application to MIT Cheetah Robot (in review)," 2013.
[30] R. S. R. Dahiya, G. Metta, M. Valle, and G. Sandini, "Tactile Sensing From Humans to Humanoids," *IEEE Transactions on Robotics*, vol. 26, no. 1, pp. 1–20, 2010.
[31] H. Yousef, M. Boukallel, and K. Althoefer, "Tactile sensing for dexterous in-hand manipulation in robotics - A review," *Sensors and Actuators A: Physical*, vol. 167, no. 2, pp. 171–187, Jun. 2011.
[32] R. Tajima, D. Honda, and K. Suga, "Fast running experiments involving a humanoid robot," *2009 IEEE International Conference on Robotics and Automation (ICRA)*, pp. 1571–1576, May 2009.
[33] D. Sadava, D. M. Hillis, H. C. Heller, and M. Berenbaum, *Life: The Science of Biology*, 3rd ed. W. H. Freeman, 2011.
[34] M. Zillich and W. Feiten, "A versatile tactile sensor system for covering large and curved surface areas," *2012 IEEE/RSJ International Conference on Intelligent Robots and Systems (IROS)*, pp. 20–24, Oct. 2012.
[35] Y. Tenzer, L. P. Jentoft, and R. D. Howe, "Inexpensive and Easily Customized Tactile Array Sensors using MEMS Barometers Chips (in review)," 2013.
[36] M. I. Tiwana, S. J. Redmond, and N. H. Lovell, "A review of tactile sensing technologies with applications in biomedical engineering," *Sensors and Actuators A: Physical*, vol. 179, pp. 17–31, Jun. 2012.
[37] M. H. Lee, "Tactile Sensing: New Directions, New Challenges," *The International Journal of Robotics Research*, vol. 19, no. 7, pp. 636–643, Jul. 2000.
[38] O. Unver and M. Sitti, "Flat dry elastomer adhesives as attachment materials for climbing robots," *Robotics, IEEE Transactions on*, vol. 26, no. 1, pp. 131–141, 2010.
[39] H. Akaike, "A new look at the statistical model identification," *IEEE Transactions on Automatic Control*, vol. 19, no. 6, pp. 716–723, 1974.
[40] R. S. Rivlin, "Large Elastic Deformations of Isotropic Materials. IV. Further Developments of the General Theory," *Philosophical Transactions of the Royal Society of London. Series A, Mathematical and Physical Sciences*, vol. 241, no. 835, pp. 379–397, Oct. 1948.
[41] E. M. Arruda and M. C. Boyce, "A three-dimensional constitutive model for the large stretch behavior of rubber elastic materials," *Journal of the Mechanics and Physics of Solids*, vol. 41, no. 2, pp. 389–412, 1993.
[42] R. W. Ogden, "Large Deformation Isotropic Elasticity - On the Correlation of Theory and Experiment for Incompressible Rubberlike Solids," *Proceedings of the Royal Society of London. A. Mathematical and Physical Sciences*, vol. 326, no. 1567, pp. 565–584, Feb. 1972.
[43] T.-F. Lu, G. C. I. Lin, and J. R. He, "Neural-network-based 3D force/torque sensor calibration for robot applications," *Engineering Applications of Artificial Intelligence*, vol. 10, no. 1, pp. 87–97, Feb. 1997.
[44] D. W. Marquardt, "An algorithm for least-squares estimation of nonlinear parameters," *Journal of the Society for Industrial and Applied Mathematics*, vol. 11, no. 2, pp. 431–441, 1963.
[45] A. Ananthanarayanan, S. Foong, and S. Kim, "A Compact Two DOF Magneto-elastomeric Force Sensor for a Running Quadruped," in *2012 IEEE International Conference on Robotics and Automation (ICRA)*, 2012, pp. 1398–1403.
[46] M. Staroswiecki, "Intelligent Sensors: A Functional View," *IEEE Transactions on Industrial Informatics*, vol. 1, no. 4, pp. 238–249, Nov. 2005.

Meng Yee (Michael) Chuah received his B.S. degree in Mechanical Engineering with a minor in Robotics in 2009 from Carnegie Mellon University, Pittsburgh, PA, and his M.S. degree in Mechanical Engineering in 2012 from Massachusetts Institute of Technology, Cambridge, MA. He is currently a Ph.D. candidate in the Biomimetic Robotics Laboratory at Massachusetts Institute of Technology. His research interests include developing sensors that are designed for, and integrated structurally into robots to enable intelligent reactions and behaviors.

Sangbae Kim received the B.S. degree from Yonsei University, Seoul, Korea, in 2001, and the M.S. and Ph.D. degrees from Stanford University, Stanford, CA, in 2004 and 2008, respectively, all in mechanical engineering. He is the Director of the Biomimetic Robotics Laboratory and an Assistant Professor of mechanical engineering at the Massachusetts Institute of Technology (MIT). He works at the convergence of mechanical engineering, biology, and material science, conducting research in the design of novel robot systems. He currently focusing on cheetah inspired robotic platform capable of high-speed gallop, employing principles from quadrupedal runners. His achievement on bioinspired technology development includes the world's first directional adhesive based on gecko lizards, and a climbing robot, Stickybot, that utilizes the directional adhesives to climb smooth surfaces. Research on the Stickybot was featured as one of the best inventions of 2006 by TIME magazine, and the papers on Stickybot won the best paper award for the Transactions on Robotics 2008 and IEEE International Conference on Robotics and Automation 2007.